Science of the Total Environment 769 (2021) 145488

Contents lists available at ScienceDirect

Science of the Total Environment

journal homepage: www.elsevier.com/locate/scitotenv

Impact of air emissions from shipping on marine phytoplankton growth

Chao Zhang [a,b], Zongbo Shi [c], Junri Zhao [d], Yan Zhang [d,*], Yang Yu [a], Yingchun Mu [e], Xiaohong Yao [a,b], Limin Feng [f], Fan Zhang [g], Yingjun Chen [d], Xiaohuan Liu [a,b], Jinhui Shi [a,b], Huiwang Gao [a,b,**]

[a] Frontiers Science Center for Deep Ocean Multispheres and Earth System, and Key Laboratory of Marine Environment and Ecology, Ministry of Education of China, Ocean University of China, Qingdao 266100, China
[b] Laboratory for Marine Ecology and Environmental Sciences, Pilot National Laboratory for Marine Science and Technology, Qingdao 266071, China
[c] School of Geography, Earth and Environmental Sciences, University of Birmingham, Birmingham B152TT, UK
[d] Shanghai Key Laboratory of Atmospheric Particle Pollution and Prevention (LAP3), Department of Environmental Science and Engineering, Fudan University, Shanghai 200092, China
[e] Estuarine and Coastal Environment Research Center, Chinese Research Academy of Environmental Sciences, Beijing 100012, China
[f] State Key Laboratory of Atmospheric Boundary Layer Physics and Atmospheric Chemistry (LAPC), Institute of Atmospheric Physics (IAP), Chinese Academy of Sciences (CAS), Beijing 100029, China
[g] Key Lab of Geographic Information Science of the Ministry of Education, School of Geographic Sciences, East China Normal University, Shanghai 200241, China

HIGHLIGHTS

- Ship-induced nitrogen deposition can lead to a predictable phytoplankton response in the surface seawater of the NWPO
- Ship emissions contribute to atmospheric nitrogen deposition in NWPO comparable to that from continent sources
- The spatial distribution of ship-enhanced primary production in the NWPO is illustrated

GRAPHICAL ABSTRACT

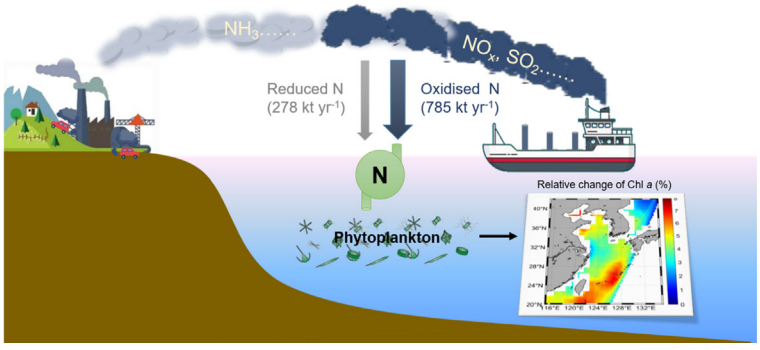

ARTICLE INFO

Article history:
Received 27 August 2020
Received in revised form 12 December 2020
Accepted 25 January 2021
Available online 30 January 2021

Editor: Julian Blasco

Keywords:
Ship emissions
Phytoplankton
Nitrogen deposition
Incubation experiment
Northwest Pacific Ocean

ABSTRACT

With the rapid expansion of maritime traffic, increases in air emissions from shipping have exacerbated numerous environmental issues, including air pollution and climate change. However, the effects of such emissions on marine biogeochemistry remain poorly understood. Here, we collected ship-emitted particles (SEPs) from the stack of a heavy-oil-powered vessel using an onboard emission test system and investigated the impact of SEPs on phytoplankton growth over the northwest Pacific Ocean (NWPO). In SEP microcosm experiments conducted in oceanic zones with different trophic statuses, the phytoplankton response, as indicated by chlorophyll *a* (Chl *a*), has been shown to increase with the proportion of SEP-derived nitrogen (N) relative to N stocks (P_{SN}) in baseline seawater, suggesting that SEPs generally promote phytoplankton growth via N fertilisation. Simulations using an air quality model combined with a ship emission inventory further showed that oxidised N (NO_x) emissions from shipping contributed ~43% of the atmospheric N deposition flux in the NWPO. Air emissions from shipping (e.g. NO_x and sulphur dioxide) also indirectly enhanced the deposition of reduced N that existed in the atmosphere, constituting ~15% of the atmospheric N deposition flux. These results suggest that the impact of airborne ship emissions on atmospheric N deposition is comparable to that of land-based emissions in the NWPO. Based on the ship-induced P_{SN} in surface seawater calculated by modeling results and World Ocean Atlas 2013 nutrient dataset, and the well-established quantitative relationship between Chl *a* and P_{SN} obtained from microcosm experiments, we found a noticeable change in surface Chl *a* concentrations due to N deposition

* Corresponding author.
** Correspondence to: H. Gao, Frontiers Science Center for Deep Ocean Multispheres and Earth System, and Key Laboratory of Marine Environment and Ecology, Ministry of Education of China, Ocean University of China, Qingdao 266100, China
E-mail addresses: yan_zhang@fudan.edu.cn (Y. Zhang), hwgao@ouc.edu.cn (H. Gao).

https://doi.org/10.1016/j.scitotenv.2021.145488

derived from marine traffic in the NWPO, particularly in the coastal waters of the Yellow Sea and open oceans. This work attempts to establish a direct link between marine productivity and air emissions from shipping.

1. Introduction

The rapid expansion of marine trade and rapid globalisation have increased the number of ships in recent years (Bencs et al., 2017). Such changes have led to continuous increases in the emissions of oxidised nitrogen (NO_x), sulphur dioxide (SO_2), oxocarbons (CO_2 and CO), volatile organic compounds (VOCs), black carbon, trace metals and particulate matter (PM), among others (Eyring et al., 2010). Considerable increases in PM and gaseous pollutants over frequently navigated waters have been observed in many studies (Eyring et al., 2010; Fan et al., 2016; Bencs et al., 2017). Such increases can alter the microphysical properties of aerosols and clouds and affect radiative forcing, ultimately influencing climate (IPCC, 2007). Ship emissions can also increase the bioavailability of nutrients such as iron (Fe) and nitrogen (N) in atmospheric deposition and potentially affect ocean biogeochemical processes (Boyd et al., 2007; Ito and Shi, 2016; Jickells et al., 2005, 2017). In general, the Fe solubility of mineral aerosols is as low as <1%, whereas that of particles emitted by the combustion of fuel can be up to 77–81% (Schroth et al., 2009). Model results have predicted that air emissions from shipping in 2100 will contribute 30–60% of the soluble iron deposition over the high-latitude North Pacific and North Atlantic (Ito, 2013). Anthropogenic emissions contribute >80% of the bioavailable N deposition to the ocean (Duce et al., 2008). More specifically, ship emissions contribute ~15% of anthropogenic NO_x globally and are becoming increasingly important in coastal areas (Corbett et al., 1999; Eyring et al., 2010; Chen et al., 2017a). The high-temperature combustion of fuel creates a suitable environment for the formation of NO_x and increases the solubility of Fe and other nutrients (Turner et al., 2017). Thus, the use of fuel to sustain intensifying levels of marine traffic for the foreseeable future will increase the importance of ships in anthropogenic emissions.

In practice, it is difficult to determine the impact of the deposition of air emissions from shipping on marine ecosystems through direct field observations. One chief reason for this is that we cannot distinguish the impact of airborne ship emissions from the impacts of other factors, such as water discharges from shipping and air emissions from continents (Jagerbrand et al., 2019). Accordingly, most previous studies have evaluated the impact of air emissions from shipping on the ocean using modeling approaches (Hunter et al., 2011; Hassellov et al., 2013; Raudsepp et al., 2019; Djambazov and Pericleous, 2015; Zhang et al., 2019). For instance, chemical modeling has shown that ship-derived emissions of NO_x and SO_2 have only a small impact on the acidification of coastal waters (i.e. in the North Sea, Baltic Sea, and South China Sea (SCS)) but could reduce the uptake of anthropogenic CO_2 in these areas (Hunter et al., 2011). Meanwhile, Hassellov et al. (2013) argued that regional pH reductions in heavily trafficked waters were of the same order of magnitude as those induced by CO_2-driven acidification. More recently, Raudsepp et al. (2019) used a coupled biochemical and physical model to simulate the impact of air emissions from shipping and found that ship-borne N deposition stimulated phytoplankton growth (e.g. diatoms, flagellates) and decreased the phosphorus (P) stock in the surface seawater of the Baltic Sea. However, their results showed that such changes induced by ship emissions had only a minor effect on the overall ecosystem. Hence, it is necessary to obtain experimental evidence to accurately assess the impact of air emissions from shipping on the marine environment and associated ecosystem.

It is well known that N stocks are generally deficient relative to P stocks in most oceanic zones (Duce et al., 2008; Moore et al., 2013; Kim et al., 2014). However, it is difficult to establish a quantitative relationship between atmospheric N input and phytoplankton response. This is because N limitation in oceanic regions characterised by varying trophic statuses can lead to different phytoplankton responses. For instance, the N input in mesotrophic to eutrophic seawater generally exerts a more pronounced stimulation effect on large phytoplankton (cell size >2 μm) than that in oligotrophic seawaters (Guo et al., 2012a; Li et al., 2015). Moreover, studies have increasingly detected the prevailing co-limitation of phytoplankton (i.e. limitation by two or more nutrients) across extensive areas of the upper oceans, especially in oligotrophic regions where nutrients are almost depleted (Moore et al., 2013; Li et al., 2015; Browning et al., 2017a; Zhang et al., 2018b). Considering the occurrence of nutrient co-limitation, the phytoplankton response to air emissions from shipping may be affected by several factors rather than N alone (Chien et al., 2016; Zhang et al., 2018b; Raudsepp et al., 2019). In addition, air emissions from shipping (a typical combustion source) typically exhibit higher trace metal solubility than mineral dust (Ito, 2013; Turner et al., 2017), which can increase the role of trace metals in affecting phytoplankton growth (Saito et al., 2008; Browning et al., 2017b). Overall, variations in the trophic statuses and phytoplankton requirements of seawater increase the difficulty in interpreting the mechanism of ship emissions in affecting marine primary production.

In recent years, the northwest Pacific Ocean (NWPO) has experienced some of the most rapid increases in shipping traffic globally (Liu et al., 2016; Zhang et al., 2017; UNCTAD, 2019). In this region, enhanced shipping traffic has markedly influenced the atmospheric composition and atmospheric deposition (Yau et al., 2012; Ito, 2013; Chen et al., 2017a, 2017b). However, its effects on the marine ecosystem of the region remain unknown. To address this gap in knowledge, the present study represents the first attempt to estimate the impact of ship-induced N deposition on primary production by combining experimental, observational, and modeling measures. The study region included coastal seas and open oceans of the NWPO: the SCS, Yellow Sea (YS), *Kuroshio* Extension (KE), and *Kuroshio–Oyashio* transition region (TR). The SCS and YS are semi-enclosed marginal seas in the NWPO. Seawater in the SCS exhibits oligotrophy characterised by nanomolar levels of N and P (Guo et al., 2012a), whereas that in the YS exhibits higher trophic statuses (even eutrophication, Liu et al., 2013). The KE exhibits variable trophic statuses, ascribed to the frequent vertical and horizontal mixing of seawater and the combined effects of the *Kuroshio* and *Oyashio* currents (Kitajima et al., 2009). The TR is influenced by the *Oyashio* current, and the concentrations of macronutrients (N and P) in TR seawater can be an order of magnitude higher than those in the KE and SCS (Measures et al., 2006; Isada et al., 2018; Zhang et al., 2020b). Considering this variability, the present study aimed to demonstrate (1) the impact of the addition of ship-emitted particles (SEPs) on phytoplankton growth in coastal seas and open oceans of the NWPO, and (2) the contribution of ship emissions to N deposition and the resultant effects on primary production in the NWPO.

2. Materials and methods

2.1. Collection of SEPs

SEP samples were collected by an onboard emission test system from the stack of the heavy-oil-powered vessel *YuKun* during a cruise undertaken on 4–13 November 2015 in the Bohai Sea (Zhang et al., 2018a, 2020a). Briefly, a sampling pipe was used to direct the ship's emissions from the stack to the particulate sampler. A flue gas analyser

was installed in the vessel exhaust pipe to test the concentration of gaseous matter. Before sampling, the flue gas was diluted 1–10 times using a dilution system. The extent of dilution was determined based on the real-time concentration of gaseous matter. Samples were collected on Teflon filters (90 mm diameter) and stored at −20 °C until laboratory analysis and onboard experiments were undertaken.

2.2. Experimental design

The protocol of the microcosm incubation experiments was designed in accordance with several previous studies (Zhang et al., 2018b, 2019a). Briefly, the surface seawater (2–5 m) for the incubation experiment was sampled on the R/V *Dongfanghong II* during two cruises in 2016 at six stations: M1 and M1B in the KE, E2 in the TR, YS1 in the YS (Cruise I: March–April), and E4 and D5 in the SCS (Cruise II: May–June, Fig. 1). Baseline seawater conditions were determined immediately after sampling, using small volumes of seawater to determine the initial concentrations of Chl *a* and nutrients (NO_3^-, NO_2^-, PO_4^{3-} and $Si(OH)_4$) at the sampling stations. The remaining sample volumes were screened through a 200 μm nylon mesh to remove large zooplankton, and then transferred evenly into acid-washed polycarbonate bottles (Nalgene), which had been rinsed thoroughly with the sampled seawater three times prior to filling. Two types of incubation bottles were used: bottles with capacities of 20 L for low-SEP additions (0.06–0.14 mg L^{-1}) and bottles with capacities of 2 L for high-SEP additions (0.59–0.70 mg L^{-1}) and various nutrient additions (each in triplicate, Table 1). The SEP loadings in this study were similar to the reportedly cumulative concentrations of atmospheric particles (0.03–0.99 mg L^{-1} over a duration of 1–30 days) in surface seawater (~10 m, Zhang et al., 2019b). Consideration of such a wide range of SEP loadings can help improve our overall understanding of the impact of SEPs on phytoplankton growth. All bottles were incubated in three large vessels where surface irradiance was attenuated by ~40%, and were maintained at relatively stable temperatures using water pumped continuously from the surface of the ocean. Incubation continued for five/six days for the 20 L bottles and four/five days for the 2 L bottles, with the total incubation time depending on the sample volume. Total (only for 2 L bottles) and size-fractionated (only for 20 L bottles) Chl *a* were sampled at 07:00–08:00 a.m. each day.

Table 1
Treatments applied to the microcosm incubation experiment.

Treatments	Stations	Added SEP concentration	Volume of incubation bottles
Control	All	No addition	20 L, 2 L
SEP-Low	E4, D5	0.07 mg L^{-1}	20 L
	M1, E2	0.08 mg L^{-1}	20 L
	M1B	0.06 mg L^{-1}	20 L
	YS1	0.14 mg L^{-1}	20 L
SEP-High	E4, D5	0.70 mg L^{-1}	2 L
	M1, E2	0.79 mg L^{-1}	2 L
	M1B	0.59 mg L^{-1}	2 L
N	All[a]	1 μmol L^{-1}	2 L
P	All	0.2 μmol L^{-1}	2 L
Fe	E2	2 nmol L^{-1}	2 L
N + P	All	1 μmol L^{-1} + 0.2 μmol L^{-1}	2 L
N + P + Fe[b]	E4, D5	1 μmol L^{-1}	20 L, 2 L
	M1, M1B, YS1	+ 0.2 μmol L^{-1} +2 nmol L^{-1}	

[a] Nutrient addition experiments were carried out in 2 L incubation bottles for all sampling stations except YS1. Only N+P+Fe additions were carried out in 20 L incubation bottles at YS1.
[b] N, P, and Fe denote $NaNO_3$, NaH_2PO_4, and $FeCl_3$, respectively.

2.3. Chemical analysis

In the land-based laboratory, the ultrasonic bath method was used to extract soluble nutrients (i.e. NO_3^-, NO_2^-, NH_4^+, PO_4^{3-}, and $Si(OH)_4$) and trace metals in the SEP samples (Zhang et al., 2019b). The extraction process lasted for 1 h at 0 °C in deionized water, followed by filtration using 0.45-μm polytetrafluoroethylene syringe filters. The extracting solution of soluble nutrients was determined immediately and that of soluble trace metals needed to be acidified by 1% HNO_3 and stored at 4 °C until analysis. In the onboard laboratory, nutrient samples from the baseline seawater (~200 mL) were gently filtered (i.e. vacuum level

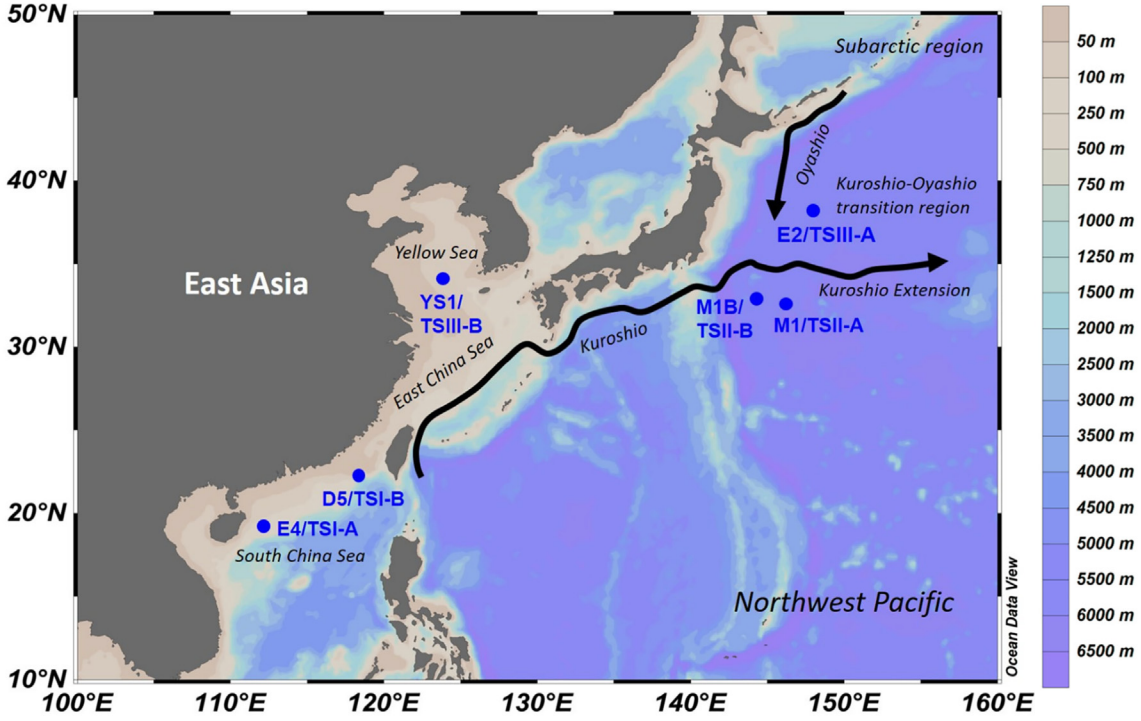

Fig. 1. Locations of the sampling stations where the onboard microcosm experiments were performed. The base map reflects water depths of the ocean.

less than or equal to 0.02 MPa) through acid-washed cellulose acetate filters (Ximengdou, China) into 125 mL polyethylene vials, and stored immediately at −20 °C until laboratory analysis of $NO_3^- + NO_2^-$, PO_4^{3-}, and $Si(OH)_4$ was conducted on land. All nutrient samples were analysed via spectrophotometric methods using the SEAL AA3 continuous flow analyser (Grasshoff et al., 1999). Soluble trace metals dissolved from SEP samples were analysed using an inductively coupled plasma mass spectrometer (ICP-MS, Agilent).

2.4. Chl a analysis

Sampled seawater collected each day from the 2 L incubation bottles was gently (i.e. vacuum level was less than or equal to 0.02 MPa) filtered through GF/F filters for total Chl *a*. For 20 L incubation bottles, sampled seawaters (collected each day) were gently filtered on 20 μm (Millipore), 2 μm (Whatman), and 0.2 μm (Whatman) filters for micro- (>20 μm), nano- (2–20 μm), and pico- (0.2–2 μm) sized Chl *a*, respectively, and total Chl *a* was calculated as the sum of Chl *a* size fractions. The sampled volume of seawater was in the range of 150–300 mL and varied depending on the total Chl *a* concentration. Immediately after filtering, the samples on the filters were transferred to dark conditions and extracted overnight in 90% acetone at −20 °C (Strickland and Parsons, 1972). Fluorescence was measured directly onboard using a Trilogy fluorometer (Turner Designs).

2.5. Descriptions of the air emission inventory for shipping and the WRF–CMAQ model

Ship emissions were estimated based on the 2015 Automatic Identification System (AIS) data following the methodology described by Fan et al. (2016) and Feng et al. (2019). The coastal/ocean-going ship emission inventories were constructed based on all shipping traffic activities and were represented in the model domain as described in Fig. S1. The non-ship emission inventory for the simulation was obtained from the 2015 national emission database (Ding et al., 2019). NO_x emissions from all anthropogenic sources and shipping traffic in the model domain were 23,673 and 1676 kt, respectively. The estimated ship-borne NO_x emissions in the model domain were within previously reported ranges of NO_x emissions within 200 nautical miles of the coastline of China. For example, values of 1381, 1443, and 1910 kt were reported by Lv et al. (2018), Li et al. (2018), and Fu et al. (2017), respectively. Discrepancies between the reported values can be attributed to (1) increased shipping traffic in 2015 relative to 2013 and differences in the geographical area considered for calculation, and (2) differences in AIS data sources and ship register databases.

The total N deposition fluxes (including oxidised and reduced N) induced by ship emissions were estimated by a combined meteorological–air quality model named the Weather Research and Forecasting (WRF, version 3.3)–Community Multiscale Air Quality (CMAQ, version 4.6) model (Daewon and Kenneth, 2006), and were based on the model results with (base case) and without (no-ship case) airborne ship emissions in 2015. A spatial resolution of 81 × 81 km was set up in this study. Additional details about the model setup and evaluation are provided in Text S1, Tables S1, and S2.

2.6. Data analysis protocol

Significant differences in the mean Chl *a* concentrations among the various experimental treatments were examined using one-way analysis of variance (ANOVA).

3. Results

3.1. Baseline surface seawater in the study regions

Broadly, the trophic status of baseline seawater increased in the following order: SCS < KE < TR < YS (Table 2). Concentrations of $NO_3^- + NO_2^-$ did not exceed 0.10 μmol L^{-1} in the SCS and increased to 0.11 μmol L^{-1} at M1B and 0.79 μmol L^{-1} at M1 in the KE. These concentrations of $NO_3^- + NO_2^-$ reached maximum values of 4.52 μmol L^{-1} at E2 in the TR and 10.70 μmol L^{-1} at YS1 in the YS. A similar pattern was observed for PO_4^{3-} and $Si(OH)_4$ (Table 2). The lowest Chl *a* concentration (≤0.14 μg L^{-1}) was also observed in the SCS, with higher values observed in the KE, TR, and YS (0.50–0.92 μg L^{-1}). Accordingly, we were able to classify the sampling stations into three distinct types based on increasing trophic status (TS), as follows: TSI (oligotrophic status)-A (E4) and TSI-B (D5) in the SCS, TSII (oligo-to-mesotrophic status)-A (M1) and TSII-B (M1B) in the KE, and TSIII (meso-to-eutrophic status)-A (E2) in the TR and TSIII-B (YS1) in the YS. This classification can help us better understand phytoplankton responses to SEP addition in seawater characterised by variable trophic statuses and provide a reference for extrapolating our results to other oceanic regions with similar characteristics.

3.2. Nutrient limitation in the study regions

Seawater in most parts of the SCS is characterised by oligotrophy (Guo et al., 2012a; Li et al., 2015; Chu et al., 2018), where nutrient concentrations (e.g. N and P) are typically extremely low, which makes it possible for nutrients to co-limit phytoplankton growth (Moore et al., 2013). In this study, the addition of N + P and N + P + Fe induced the most significant increases in Chl *a* relative to those of the control and single-nutrient treatments ($p < 0.05$) at TSI-A (days 3–5) and TSI-B (days 4–5, Fig. 2). We found there was no significant difference in Chl *a* between the N + P and N + P + Fe treatments ($p > 0.05$), indicating no Fe limitation of phytoplankton. In the single-nutrient treatments, the addition of N at TSI-A, and N or P at TSI-B induced significant differences ($p < 0.05$) in Chl *a* relative to that of the control, while the maximum Chl *a* concentrations were only 24–44% of those in the N + P treatments. Therefore, we conclude that phytoplankton at TSI-A and

Table 2
Baseline conditions at the sampling stations.

	E4/TSI-A	D5/ TSI-B	M1/TSII-A	M1B/ TSII-B	E2/ TSIII-A	YS1/ TSIII-B
Sampling date	2016.5.30	2016.6.5	2016.3.28	2016.4.18	2016.4.3	2016.3.22
Incubation duration	5 days (20 *L*, 2*L*)	6 days (20*L*) 5 days (2 L)	5 days (20 L) 4 days (2 L)	5 days (20 L) 4 days (2 L)	6 days[b] (20 L) 5 days (2 L)	5 days (20 L)
Location	19.1°N, 112.3°E	22.0°N, 118.4°E	32.4°N, 146.3°E	32.8°N, 144.2°E	38.0°N, 148.1°E	34.0°N, 123.9°E
Region	SCS	SCS	KE	KE	TR	YS
Chl *a*[a] (μg L^{-1})	0.09	0.14	0.76	0.50	0.63	0.92
$NO_3^- + NO_2^-$ (μmol L^{-1})	0.06	0.09	0.79	0.11	4.52	10.70
PO_4^{3-} (μmol L^{-1})	0.02	0.03	0.10	0.05	0.35	0.67
$Si(OH)_4$ (μmol L^{-1})	1.72	1.28	2.19	1.42	6.12	14.99

[a] Total Chl *a* concentration was calculated as the sum of Chl *a* concentrations for each size fraction.
[b] The sampled seawater was not collected from the 20 L incubation bottles on day 5 owing to a hostile marine environment.

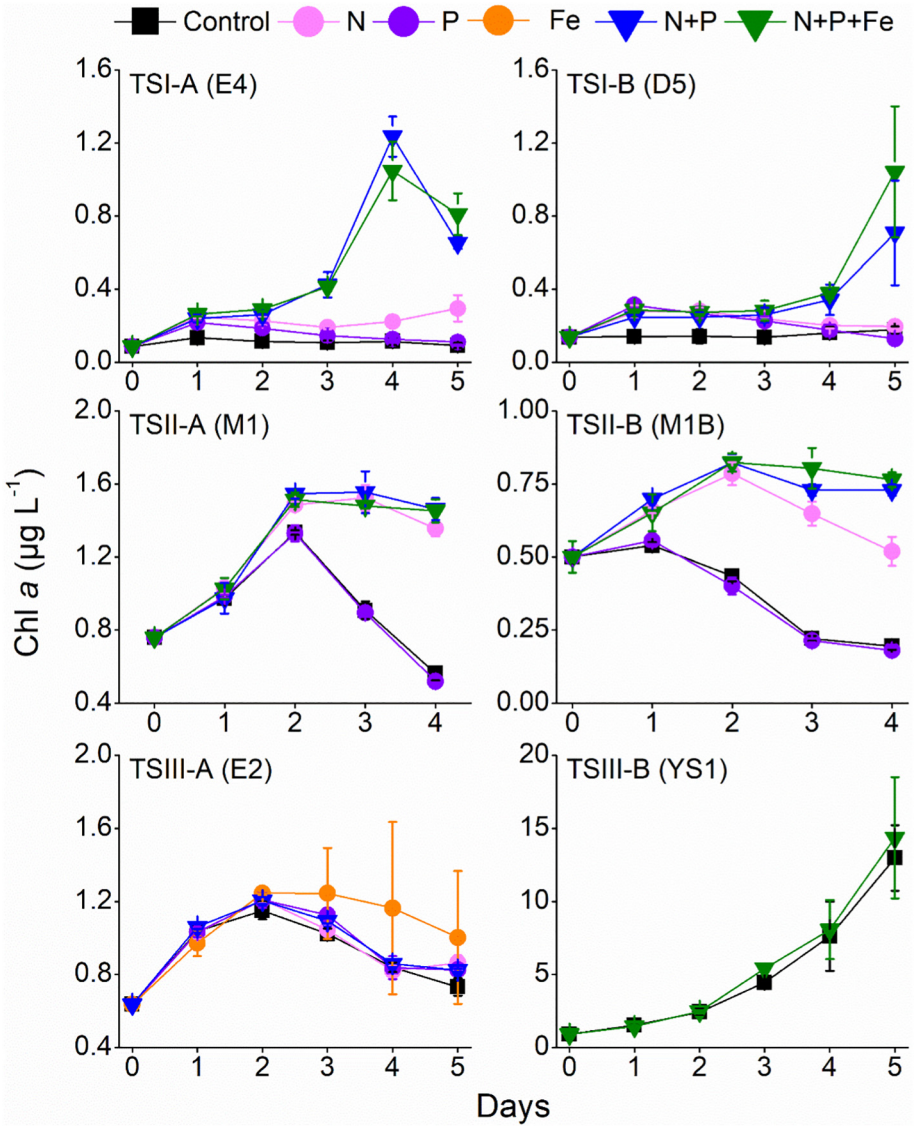

Fig. 2. Responses of Chl *a* concentrations to various nutrient additions over the duration of the incubation experiments. "Control", "N", "P", "Fe", "N + P", and "N + P + Fe" in this figure indicate the control, N, P, Fe, N + P, and N + P + Fe treatments, respectively.

TSI-B are co-limited by N and P, with N being the primary limiting nutrient.

In the KE, both the *Kuroshio* water from the southwest and the *Kuroshio–Oyashio* transition water from the north are characterised by N:$P < 16$, which generally leads to an excess of P relative to N in seawater (Whitney, 2011; Guo et al., 2012b). In our study, the additions of N, N + P, and N + P + Fe induced the most significant increases in Chl *a* relative to those of the control and P-only treatments ($p < 0.05$) at TSII-A and TSII-B (days 2–4, Fig. 2). We found no significant difference in Chl *a* in the N, N + P, and N + P + Fe treatments at TSII-A ($p > 0.05$) and found a significant difference between the N + P/N + P + Fe and N treatments at TSII-B on only one day (day 4). This indicates that phytoplankton were limited primarily by N at both TSII-A and TSII-B.

At TSIII-A in the TR, the addition of Fe induced an increase in Chl *a* compared with that of the control and other nutrient (N, P, N + P) treatments (Fig. 2), indicating phytoplankton were likely limited by Fe. This result is consistent with previous studies showing that low availability of Fe is typical of this region (Noiri et al., 2005; Isada et al., 2018). At TSIII-B in the YS, only the N + P + Fe addition experiment was conducted, and we did not find a significant difference relative to the control ($p > 0.05$, Fig. 2). In addition, Chl *a* increased noticeably in the control during the incubation experiments, indicating the occurrence of a bloom (Liu et al., 2013). From this, in conjunction with the replete nutrient stocks of the baseline seawater, we infer that phytoplankton at TSIII-B were not limited by N, P, Fe, or their combinations. In the YS, various factors can supply replete nutrients to cause annual spring bloom of phytoplankton. These factors include riverine inputs, atmospheric deposition, frequent upwelling of waters due to low water depth (generally <100 m) and strong wind stress, and accumulation of nutrients in winter (Liu et al., 2003; Ren et al., 2011; Liu et al., 2013).

3.3. Response of phytoplankton to SEP addition

The actual concentrations of the SEP components added to the incubated seawater can be calculated by adding the masses of the SEPs per litre of seawater (Table 3). Generally, SEPs provided dissolved inorganic N (DIN, including NO_3^-, NO_2^-, and NH_4^+), various trace metals (especially Fe, Co, Ni, and Zn), and negligible amounts of PO_4^{3-} and $Si(OH)_4$, according to the Redfield ratio and the characteristics of the baseline seawater (Table 2). At TSI-A and TSI-B in the SCS, the addition of low and high SEPs markedly increased the concentrations of DIN (i.e. by 14–243% relative to the baseline seawater, Fig. 3a). Accordingly, the maximum concentrations of Chl *a* for the low and high SEP treatments at TSI-A were

Table 3
Amounts of macro- and micro-nutrients (soluble trace metals) added for the low and high SEP treatments.

Added amount (mg L^{-1})	Macro-nutrients (nmol L^{-1})			Micro-nutrients (ng L^{-1})							
	DIN[a]	$Si(OH)_4$	PO_4^{3-}	Cr	Mn	Fe	Co	Ni	Cu	Zn	V	Pb
0.14-YS	29.10	0.18	1.16	2.64	15.62	160.98	25.11	624.60	10.51	43.31	447.81	1.41
0.06/0.59-M1B	12.47/122.61	0.08/0.76	0.50/4.91	1.13/11.3	6.70/65.8	68.99/678.4	10.76/105.8	267.68/2632.2	4.50/44.3	18.56/182.52	191.92/1887.2	0.60/5.94
0.07/0.7-E4, D5	14.55/145.48	0.09/0.90	0.58/5.82	1.32/13.2	7.81/78.1	80.49/804.9	12.55/125.5	312.30/3123.0	5.25/52.54	21.66/216.6	223.90/2239.0	0.70/7.0
0.08/0.79-M1, E2	16.63/164.18	0.10/1.02	0.67/6.57	1.51/14.9	8.92/88.1	91.99/908.4	14.35/141.7	356.91/3524.5	6.00/59.3	24.75/244.4	255.89/2526.9	0.80/8.0

[a] Dissolved inorganic nitrogen (DIN) is regarded as the sum of NO_3^-, NO_2^-, and NH_4^+.

~1.2- and ~1.5-fold higher than those for the control experiments, respectively (Fig. 3b). Similar phytoplankton responses were also observed at TSI-B. At TSII-A and TSII-B in the KE, the considerable supply of DIN from high-SEP additions increased the maximum Chl *a* significantly (~1.2- and ~1.4-fold) relative to those of the controls. The contribution of DIN supplied by low-SEP additions was found to be 11% of that of the baseline at TSII-B, and thus the maximum Chl *a* was found to be only 1.1-fold higher than that of the control (Fig. 3b). At TSII-A, we found no significant difference in Chl *a* between the control and low-SEP treatments ($p < 0.05$), which we attribute to the negligible input of DIN by low-SEP additions (Fig. 3). At the TSIII stations, nutrient concentrations were relatively replete, and only the high-SEP additions at TSIII-A induced a significant increase ($p < 0.05$) in Chl *a* relative to that of the control (Fig. 3b).

3.4. Impact of airborne ship emissions on N deposition over the NWPO

In general, the total N deposition flux induced by all anthropogenic sources and ship emissions (ship-derived N) showed a similar trend of spatial distribution, i.e. decreasing N deposition flux with increasing distance from the coastline (Fig. 4a and b). The opposite trend was observed in the relative contribution of ship emissions to the total N deposition flux induced by all anthropogenic sources (Fig. 4c). The ship-induced N deposition flux in the model domain was up to 1.3 g m^{-2} yr^{-1} (Fig. 4b). This is similar to the highest value of 1 g m^{-2} yr^{-1} simulated by Chen et al. (2020). The annual amount of total N deposition flux was 1841 kt in 2015. Of this, 1063 kt was associated with air emissions from shipping (~58%). The ship-induced N deposition included the oxidised N deposition of 785 kt formed directly from ship-emitted NO_x and the indirectly enhanced reduced N deposition of 278 kt due to chemical reactions with ambient NH_3 (Table 4). The indirect shipping-enhanced deposition of reduced N in different seasons accounts for 21–49% of the direct shipping-enhanced deposition of oxidised N (Table 4).

4. Discussion

4.1. Fertilisation effects of SEP on phytoplankton growth

On the basis of the phytoplankton response to nutrient and SEP enrichment, we found that the input of N by SEP addition was the primary factor responsible for phytoplankton growth at stations TSI and TSII. This was also supported by the positive correlation between the proportion of N supplied by SEPs relative to N stocks in the baseline seawater (i.e. P_{SN} = [N supplied by SEP additions/N stocks in the baseline seawater] × 100) and the extent of the phytoplankton response (i.e. $RC_{Chl\ a}$ = [Mean in the SEP treatments - Mean in the control]/Mean in the control) × 100, Fig. 5a) in the incubated seawater. The importance of N deposition in primary production has been demonstrated in China's coastal seas (Guo et al., 2012a; Shi et al., 2012) and open oceans of the NWPO (Martino et al., 2014; Zhang et al., 2019b). This is ascribed to increasing anthropogenic N emissions in East Asia (Kim et al., 2014) and primarily N limitation in most regions of the NWPO on the basis of field observations (Duce et al., 2008; Okin et al., 2011), in-situ experiments (Li et al., 2015; Zhang et al., 2019b) and modeling (Dutkiewicz et al., 2012). We note that the slope of the relationship between $RC_{Chl\ a}$ and P_{SN} decreases gradually with increasing P_{SN}, suggesting that the effects of N nutrients on phytoplankton growth wane with the gradual alleviation of the pressures exerted by N shortage. Although N is the primary limiting nutrient, the stocks of other biologically essential nutrients in incubated seawater also affect phytoplankton growth (Moore et al., 2013; Zhang et al., 2019a). Moreover, a switch in the most deficient nutrient can occur with alteration of the nutrient structure in seawater under the influence of substantial N input (Arrigo, 2005; Zhang et al., 2018b).

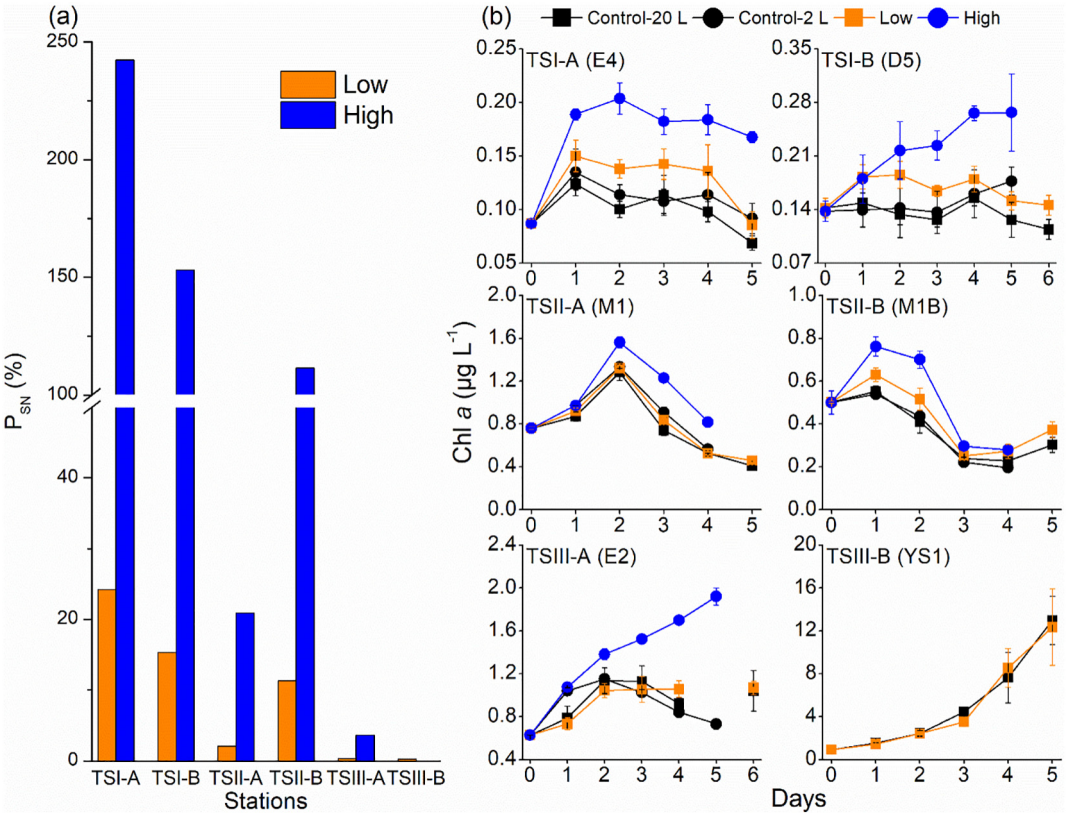

Fig. 3. (a) Proportion of N supplied by ship-emitted particles (SEPs) relative to N stocks in the baseline seawater (P_{SN} = [N supplied by SEP additions/N stocks in the baseline seawater] × 100) for low and high SEP treatments at the sampling stations. (b) Responses of total Chl *a* to low and high SEP additions during the incubation experiments. "Control-20 L" and "Control-2 L" indicate the control treatments for 20 L and 2 L incubation bottles, respectively. "Low" and "High" indicate low-SEP treatments and high-SEP treatments, respectively.

Although the added amounts of N and/or P in the nutrient treatments were far higher than those in the SEP treatments (Tables 1 and 3), the results for these nutrient treatments provide a useful reference to interpret the phytoplankton response to SEP addition at stations TSI and TSII to some extent. In general, the $RC_{Chl\ a}$ induced by SEP addition was initially similar to that in the nutrient treatments (i.e. N, N + P, and N + P + Fe), and then, with increasing P_{SN} (as extended from the fitted curve), the $RC_{Chl\ a}$ values gradually ranged between those in the N and N + P/N + P + Fe treatments (Fig. 5b). The N supplied by SEP addition in the present study played a key role in stimulating phytoplankton growth owing to the negligible supply of P. This corresponded to similar phytoplankton responses in the N, N + P, and N + P + Fe treatments at TSII-A (P_{SN} = 127%, Fig. 5b). With increases in P_{SN}, the amount of P added by SEP addition relative to that of the baseline seawater is no longer negligible, and thus, the increases in Chl *a* associated with the SEP treatments are higher than those associated with the N-only treatment (Fig. 5b). Input of P can promote cell division, which can potentially increase the Chl *a* concentration by increasing the number of cells (Cavender-Bares et al., 1999; Arrigo, 2005). Meanwhile, when we supposed that 1 μmol L^{-1} of N was supplied by SEP addition, the calculated amount of P added (~0.04 μmol L^{-1}) was much lower than that in the P-only treatment (0.2 μmol L^{-1}). Therefore, the addition of N + P and

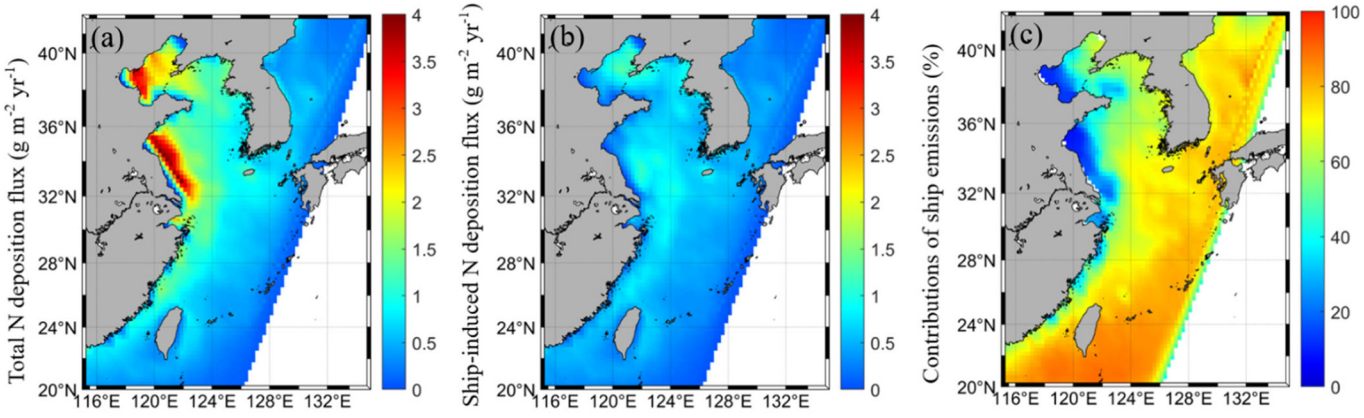

Fig. 4. Annual N (including oxidised N and reduced N) deposition fluxes in the northwest Pacific Ocean from (a) all anthropogenic sources, (b) ship emissions, and (c) contributions of ship emissions to the annual N deposition fluxes.

Table 4
Seasonal and annual N deposition fluxes induced by ship emissions and all anthropogenic sources (kt N yr^{-1}).

Seasons	All anthropogenic sources			Ship-induced oxidised N deposition (Direct)	Ship-induced reduced N deposition (Indirect)	Contribution (%) of ship-induced oxidised N deposition to total N deposition	Contribution (%) of ship-induced reduced N deposition to total N deposition
	Total N deposition	Oxidised N deposition	Reduced N deposition				
Spring	417.1	237.0	180.1	178.2	63.4	42.7	15.2
Summer	360.7	220.1	140.6	162.8	35.3	45.1	9.8
Autumn	418.3	255.1	163.2	176.8	48.4	42.2	11.6
Winter	644.6	359.5	285.0	267.2	130.9	41.4	20.3
Annual	1840.7	1071.8	768.9	785.0	278.1	42.6	15.1

N + P + Fe induced larger increases in Chl *a* than the SEP treatments, as observed at TSI-A and TSI-B (Fig. 5b).

On the other hand, SEP addition supplied considerable amounts of trace metals such as Zn and/or Fe (Table 3), which have the potential to facilitate the utilisation of dissolved organic matter as a P source by phytoplankton under P limitation. Such enhancement of the use of dissolved organic P, induced by atmospheric deposition, has been widely reported in previous studies (Moore et al., 2013; Browning et al., 2017b; Chu et al., 2018). Hence, although SEP-derived N was the primary factor stimulating phytoplankton growth in our study, the impact of P and trace metals may be important when P_{SN} is sufficiently large, especially in the oligotrophic seawater that constitutes ~60% of the global ocean (Longhurst et al., 1995).

At TSIII-A in the TR, the addition of low and high SEP supplied ~1.6 and ~ 16 nmol Fe L^{-1} to the incubated seawater, respectively. However, a significant increase in Chl *a* was observed only for the high treatments (Fig. 3b). Other trace metals supplied by SEP addition, such as Zn and Co, might also affect phytoplankton growth in the North Pacific (Table 3, Crawford et al., 2003; Saito et al., 2008; Jakuba et al., 2012). Because of the experimental conditions, our onboard incubation experiments did not strictly follow the 'trace metal clean' technique. Accordingly, we could not directly verify the role of each trace metal in phytoplankton growth. However, it is clear that a considerable input of SEPs can have a significant fertilisation effect on phytoplankton growth in the TR (Fig. 3b). At TSIII-B in the YS, the negligible difference in Chl *a* between the control and SEP treatments is largely due to the baseline nutrient-replete condition that has created an ideal environment for phytoplankton growth (Fig. 3b, Table 2).

4.2. Characteristics of ship-induced N deposition

In our study, although ship-borne NO_x emissions in the model domain account for only 7.1% of the total NO_x emissions, up to 97% of ship-borne NO_x could be deposited over the ocean. Hence, the direct contribution of airborne ship emissions to total N deposition could be approximately 43% in this domain (Table 4). Indeed, compared with the rapid decrease in the deposition rates of terrestrial anthropogenic N observed with increasing distance from the East Asian continent (Kim et al., 2014), the sustained emissions associated with shipping play an increasingly important role in N deposition flux over the ocean (Jickells et al., 2017). Moreover, the relative contribution of ship-borne NO_x may increase in the near future, with further NO_x reductions from power plants and land traffic. Some overestimations are present in the relative contribution of shipping. In particular, this

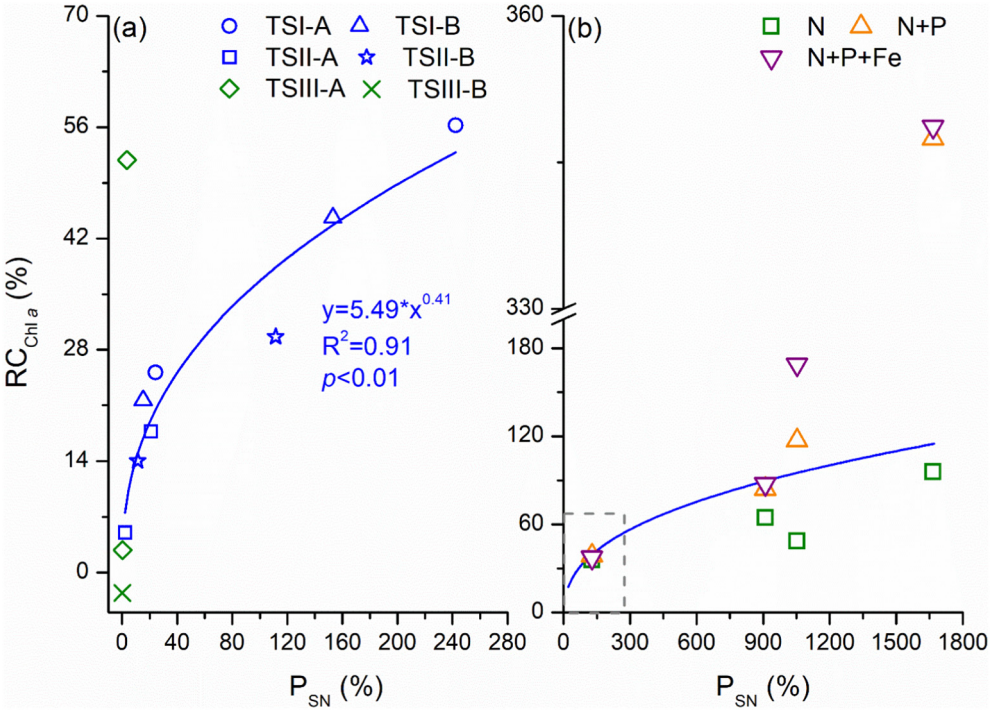

Fig. 5. Relationships between relative change in Chl *a* ($RC_{Chl\ a}$, ([Mean in the ship emitted particle (SEP) treatments-Mean in the control]/Mean in the control) × 100) and proportion of N supplied by SEPs relative to N stocks in the baseline seawater (P_{SN}, [N supplied by SEP additions/N stocks in the baseline seawater] × 100) for (a) SEP and (b) nutrient (N, N + P, and N + P + Fe) treatments. The olive open symbols in Fig. (a) were obtained from SEP treatments at TSIII-A (E2, Fe limitation) and TSIII-B (YS1, no limitation of N, P, Fe), which were not used to fit the curve. In (b), the dashed panel region corresponds to the fitted curve in (a), and the line out of the dashed panel was extended from the fitted curve (a). The P_{SN} (x-axis) in (b) corresponds, in increasing order, to stations TSII-A (M1), TSII-B (M1B), TSI-B (D5), and TSI-A (E4).

study considered terrestrial NO_x emissions from only China, excluding other areas of Southeast Asia such as Japan and Korea. However, statistical estimates according to the simulation results suggest that approximately 10% of N originating from other terrestrial sources (i.e. excluding China) is deposited over the ocean. Thus, the net effect of overestimation is likely limited.

In addition, we note that shipping traffic indirectly enhanced the deposition of reduced N (Table 4). Previous studies focussed primarily on the contribution of ship-borne NO_x to N deposition (Jagerbrand et al., 2019; Raudsepp et al., 2019; Zhang et al., 2019; Chen et al., 2020). However, our study indicates that the impact of ship emissions on reduced N deposition should not be neglected in future studies. This is because the direct emissions of ship-borne NO_x and SO_2 have the potential to enhance the efficiency of NH_4^+ deposition under saturated NH_4^+ conditions.

4.3. Impact of ship-induced N deposition on surface Chl a changes over the NWPO

The good nonlinear relationship between P_{SN} and $RC_{Chl\ a}$ obtained from the onboard incubation experiments enlightens us to evaluate the general impact of airborne ship emissions on surface Chl *a* changes over the NWPO. Considering the previously published N residence time for coastal waters over one year (Galloway et al., 2003; Boyer and Howarth, 2013), increases in the DIN concentrations in surface seawater induced by ship emissions were estimated using the ship-induced N deposition fluxes (unit: g m^{-2} yr^{-1}) divided by an annually mixed layer depth (unit: m). The baseline DIN concentration in surface seawater was obtained from the World Ocean Atlas (WOA) 2013 nutrient dataset. Therefore, we could illustrate the spatial distribution of $RC_{Chl\ a}$ over the NWPO on the basis of calculated P_{SN}.

As shown in Fig. 6, the $RC_{Chl\ a}$ values induced by airborne ship emissions ranged from 1.0% to 7.1% (4.2% on average). The model results for the Baltic Sea also showed that the relative change in phytoplankton productivity (unit: mmol N m^{-3}) induced by ship-borne nutrients (dominated by atmospheric N deposition) was no larger than 10% (Raudsepp et al., 2019). Noticeable increases in Chl *a* concentration

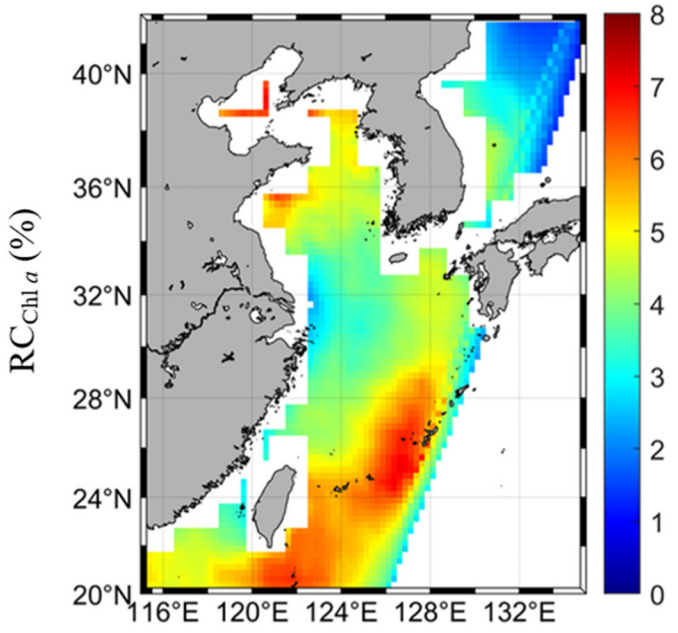

Fig. 6. Relative change in Chl *a* ($RC_{Chl\ a}$) in surface seawater owing to ship-induced N deposition. $RC_{Chl\ a}$ was based on the empirical equation obtained from the incubation experiments as shown in Fig. 5a. The results in this figure were obtained by excluding the area where N:P ratios in the surface seawater exceeded 16:1 according to the World Ocean Atlas 2013 nutrient dataset.

were observed in the coastal waters of the YS and open oceans of the NWPO (Fig. 6). This pattern of change is distinct from the spatial distribution of ship-induced N deposition over the ocean (Fig. 4b, Chen et al., 2020), because N stocks in surface seawater also affect the phytoplankton response to external nutrient inputs (Noiri et al., 2005; Meng et al., 2016; Zhang et al., 2020a, b). Note that lower $RC_{Chl\ a}$ values were observed in the eastern parts of the ECS, where seawater is characterised by eutrophication due to the influence of the Yangtze diluted water. However, the absolute accumulation of Chl *a* could be even larger in this region because of the higher stocks of phytoplankton biomass that are present (Meng et al., 2016; Zhang et al., 2019a). In addition, atmospheric deposition may have altered the phytoplankton community while having a negligible effect on the Chl *a* concentration (Meng et al., 2016).

Our estimates did not include regions for which the N:P ratio in surface seawater exceeded 16:1 (corresponding primarily to nearshore regions), because we considered that phytoplankton were limited primarily by P under these conditions according to the Redfield ratio (Duce et al., 2008; Moore et al., 2013). However, phytoplankton have the ability to trigger acclimatisation mechanisms to cope with P limitation. Such mechanisms include increasing the N:P stoichiometry and utilising dissolved organic phosphorus (Arrigo, 2005; Moore et al., 2013; Zhang et al., 2019a). In addition, ship-induced N deposition likely has a supplementary stimulation impact on phytoplankton, even if N is not the primary limiting nutrient (Zhang et al., 2019a). Hence, the actual area influenced by ship-induced N deposition in the NWPO may not be confined to the N-limiting regions. Further study is needed to encompass the whole ocean and consider areas characterised by variable nutrient-limiting conditions.

5. Conclusions

In this study, we conducted a series of microcosm experiments to elucidate the overall fertilisation effects of SEP addition on phytoplankton growth. By establishing a quantitative relationship between P_{SN} and $RC_{Chl\ a}$ on the basis of in-situ microcosm experiments, the phytoplankton response to ship-induced N deposition in the NWPO has become predicable to some extent. The WRF–CMAQ model was used to estimate the N deposition flux induced by ship emissions in 2015, and demonstrated the important contribution of ship emissions to the total N deposition flux (~58%) over the NWPO. The P_{SN} induced by airborne ship emissions in the surface seawater of the NWPO was obtained by combining ship-induced N deposition flux from the model results and DIN concentrations from the WOA dataset. Accordingly, we found a noticeable impact of airborne ship emissions on phytoplankton growth indicated by $RC_{Chl\ a}$ in both coastal waters and open oceans of the NWPO. In contrast to open oceans, coastal waters characterised by higher biomasses are more favourable for fixing carbon at the same value of $RC_{Chl\ a}$. Meanwhile, large phytoplankton with higher sinking rates, generally have higher biomass contributions in coastal waters, and thus are favourable for increasing the export efficiency of fixed carbon due to airborne ship emissions (Maranon, 2015; Zhang et al., 2020b). Considering the widespread distribution of N-limited regions in the global ocean (Moore et al., 2013) and the rapid spread and deposition of substances emitted in association with worldwide shipping traffic, we posit that the impact of SEPs on marine production may extend to other similar oceanic regions. We foresee an increase in the importance of ship emissions in marine biogeochemical cycles in the near future and suggest that combining multiple measures (including field observations, modeling, and remote sensing) will be necessary to evaluate this impact globally.

Data and materials availability

Relevant data are reported in the text or supplementary material, and data in tables are available on request.

CRediT authorship contribution statement

Chao Zhang: Conceptualization, Formal analysis, Investigation, Methodology, Visualization, Writing – original draft, Funding acquisition. **Zongbo Shi:** Conceptualization, Formal analysis, Writing – review & editing, Supervision, Funding acquisition. **Junri Zhao:** Data curation, Investigation, Resources. **Yan Zhang:** Formal analysis, Methodology, Resources, Writing – review & editing, Supervision, Funding acquisition. **Yang Yu:** Data curation, Visualization. **Yingchun Mu:** Investigation. **Xiaohong Yao:** Data curation, Writing – review & editing. **Limin Feng:** Investigation. **Fan Zhang:** Investigation. **Yingjun Chen:** Resources. **Xiaohuan Liu:** Data curation. **Jinhui Shi:** Resources. **Huiwang Gao:** Conceptualization, Methodology, Writing – review & editing, Supervision, Funding acquisition.

Declaration of competing interest

The authors declare no competing conflict of interest.

Acknowledgments

This work was funded by National Natural Science Foundation of China (NSFC) (41876125: Gao; 41906119: Zhang C.; 21677038: Zhang Y.), NSFC and Royal Society travel grant (4141101141: Gao and Shi), NSFC-Shandong Joint Fund (U1906215: Gao), Major State Basic Research Development Program of China (973 Program) (2014CB953701: Gao). Shi is also supported by the Natural Environment Research Council (NE/S00579X/1). We thank the open research cruise NORC2015-05 supported by NSFC Shiptime Sharing Project (project number: 41449905) for supporting the microcosm incubation experiments.

Appendix A. Supplementary data

Supplementary data to this article can be found online at https://doi.org/10.1016/j.scitotenv.2021.145488.

References

Arrigo, K.R., 2005. Marine microorganisms and global nutrient cycles. Nature. 437 (7057), 349–355. https://doi.org/10.1038/nature04158.

Bencs, L., Horemans, B., Buczynska, A.J., Van, G.R., 2017. Uneven distribution of inorganic pollutants in marine air originating from ocean-going ships. Environ. Pollut. 222, 226–233. https://doi.org/10.1016/j.envpol.2016.12.052.

Boyd, P.W., Jickells, T., Law, C., Blain, S., Boyle, E., Buesseler, K., Coale, K., Cullen, J., De Baar, H., Follows, M., 2007. Mesoscale iron enrichment experiments 1993–2005: synthesis and future directions. Science. 315 (5812), 612–617. https://doi.org/10.1126/science.1131669.

Boyer, E.W., Howarth, R.W. (Eds.), 2013. The Nitrogen Cycle at Regional to Global Scales. Springer Science & Business Media.

Browning, T.J., Achterberg, E.P., Rapp, I., Engel, A., Bertrand, E.M., Tagliabue, A., Moore, C.M., 2017a. Nutrient co-limitation at the boundary of an oceanic gyre. Nature. 551 (7679), 242. https://doi.org/10.1038/nature24063.

Browning, T.J., Achterberg, E.P., Yong, J.C., Rapp, I., Utermann, C., Engel, A., Moore, C.M., 2017b. Iron limitation of microbial phosphorus acquisition in the tropical North Atlantic. Nat. Commun. 8 (1), 15465. https://doi.org/10.1038/ncomms15465.

Cavender-Bares, K.K., Mann, E.L., Chisholm, S.W., Ondrusek, M.E., Bidigare, R.R., 1999. Differential response of equatorial Pacific phytoplankton to iron fertilization. Limnol. Oceanogr. 44 (2), 237–246. https://doi.org/10.4319/lo.1999.44.2.0237.

Chen, D., Wang, X., Li, Y., Lang, J., Zhou, Y., Guo, X., Zhao, Y., 2017a. High-spatiotemporal-resolution ship emission inventory of China based on AIS data in 2014. Sci. Total Environ. 609, 776–787. https://doi.org/10.1016/j.scitotenv.2017.07.051.

Chen, D., Wang, X., Nelson, P., Li, Y., Zhao, N., Zhao, Y.H., Lang, J.L., Zhou, Y., Guo, X.R., 2017b. Ship emission inventory and its impact on the $PM_{2.5}$ air pollution in Qingdao Port, North China. Atmos. Environ. 166, 351–361. https://doi.org/10.1016/j.atmosenv.2017.07.021.

Chen, D., Fu, X., Guo, X., Lang, J., Zhou, Y., Li, Y., Liu, B., Wang, W., 2020. The impact of ship emissions on nitrogen and sulfur deposition in China. Sci. Total Environ. 708, 134636. https://doi.org/10.1016/j.scitotenv.2019.134636.

Chien, C.T., Mackey, K.R., Dutkiewicz, S., Mahowald, N.M., Prospero, J.M., Paytan, A., 2016. Effects of African dust deposition on phytoplankton in the western tropical Atlantic Ocean off Barbados. Global Biogeochem. Cy. 30 (5), 716–734. https://doi.org/10.1002/2015GB005334.

Chu, Q., Liu, Y., Shi, J.H., Zhang, C., Gong, X., Yao, X.H., Guo, X.Y., Gao, H.W., 2018. Promotion effect of Asian dust on phytoplankton growth and potential dissolved organic phosphorus utilization in the South China Sea. J. Geophys. Res.-Biogeo. 123 (3), 1101–1116. https://doi.org/10.1002/2017JG004088.

Corbett, J.J., Fischbeck, P.S., Pandis, S.N., 1999. Global nitrogen and sulfur inventories for oceangoing ships. J. Geophys. Res.-Atmos. 104 (D3), 3457–3470. https://doi.org/10.1029/1998JD100040.

Crawford, D.W., Lipsen, M.S., Purdie, D.A., Lohan, M.C., Statham, P.J., Whitney, F.A., Putland, J.N., Johnson, W.K., Sutherland, N., Peterson, T.D., Harrison, P.J., Wong, C.S., 2003. Influence of zinc and iron enrichments on phytoplankton growth in the northeastern subarctic Pacific. Limnol. Oceanogr. 48 (4), 1583–1600. https://doi.org/10.4319/lo.2003.48.4.1583.

Daewon, B., Kenneth, L.S., 2006. Review of the governing equations, computational algorithms, and other components of the models-3 community multiscale air quality (cmaq) modeling system. Appl. Mech. Rev. 59 (2), 51–77. https://doi.org/10.1115/1.2128636.

Ding, D., Xing, J., Wang, S., Liu, K., Hao, J., 2019. Estimated contributions of emissions controls, meteorological factors, population growth, and changes in baseline mortality to reductions in ambient $PM_{2.5}$ and $PM_{2.5}$-related mortality in China, 2013–2017. Environ. Health Persp. 127 (6), 067009. https://doi.org/10.1289/EHP4157.

Djambazov, G., Pericleous, K., 2015. Modelled atmospheric contribution to nitrogen eutrophication in the English Channel and the southern North Sea. Atmos. Environ. 102, 191–199. https://doi.org/10.1016/j.atmosenv.2014.11.071.

Duce, R.A., La Roche, J., Altieri, K., Arrigo, K.R., Baker, A.R., Capone, D.G., Cornell, S., Dentener, F., Galloway, J., Ganeshram, R.S., Geider, R.J., Jickells, T., Kuypers, M.M., Langlois, R., Liss, P.S., Liu, S.M., Middleburg, J.J., Moore, C.M., Nickovic, S., Oschlies, A., Pedersen, T., Prospero, J., Schlitzer, R., Seitzinger, S., Sorensen, L.L., Uematsu, M., Ulloa, O., Voss, M., Ward, B., Zamora, L., 2008. Impacts of atmospheric anthropogenic nitrogen on the open ocean. Science. 320 (5878), 893–897. https://doi.org/10.1126/science.1150369.

Dutkiewicz, S., Ward, B.A., Monteiro, F., Follows, M.J., 2012. Interconnection of nitrogen fixers and iron in the Pacific Ocean: theory and numerical simulations. Global Biogeochem. Cy. 26 (1). https://doi.org/10.1029/2011GB004039.

Eyring, V., Isaksen, I.S., Berntsen, T., Collins, W.J., Corbett, J.J., Endresen, O., Grainger, R.G., Moldanova, J., Schlager, H., Stevenson, D., 2010. Transport impacts on atmosphere and climate: shipping. Atmos. Environ. 44 (37), 4735–4771. https://doi.org/10.1016/j.atmosenv.2009.04.059.

Fan, Q., Zhang, Y., Ma, W., Ma, H., Feng, J., Yu, Q., Yang, X., Simon, K., Chen, L., 2016. Spatial and seasonal dynamics of ship emissions over the Yangtze River Delta and East China Sea and their potential environmental influence. Environ. Sci. Technol. 50 (3), 1322–1329. https://doi.org/10.1021/acs.est.5b03965.

Feng, J., Zhang, Y., Li, S., Mao, J., Patton, A. P., Zhou, Y., Ma, W., Liu, C., Kan, H., Huang, C., An, J., Li, L., Shen, Y., Fu , Q., Wang, X., Liu, J., Wang, S., Ding. D., Chen, J., Ge, W., Zhu., H., Walker, K., 2019. The influence of spatiality on shipping emissions, air quality and potential human exposure in the Yangtze River Delta/Shanghai, China. Atmos. Chem. Phys. 19(9), 6167–6183. doi:https://doi.org/10.5194/acp-19-6167-2019.

Fu, M., Liu, H., Jin, X., He, K., 2017. National-to port-level inventories of shipping emissions in China. Environ. Res. Lett. 12 (11), 114024. https://doi.org/10.1088/1748-9326/aa897a.

Galloway, J.N., Aber, J.D., Erisman, J.W., Seitzinger, S.P., Howarth, R.W., Cowling, E.B., Cosby, B.J., 2003. The nitrogen cascade. Bioscience. 53 (4), 341–356. https://doi.org/10.1641/0006-3568(2003)053.

Grasshoff, K., Kremling, K., Ehrhardt, M., 1999. Methods of Seawater Analysis. 3 edn. Wiley-VCH.

Guo, C., Yu, J., Ho, T.-Y., Wang, L., Song, S., Kong, L., Liu, H., 2012a. Dynamics of phytoplankton community structure in the South China Sea in response to the East Asian aerosol input. Biogeosciences. 9 (4), 1519–1536. https://doi.org/10.5194/bg-9-1519-2012.

Guo, X., Zhu, X., Wu, Q., Huang, D., 2012b. The Kuroshio nutrient stream and its temporal variation in the East China Sea. J. Geophys. Res.-Oceans. 117, C01026. https://doi.org/10.1029/2011JC007292.

Hassellov, I.M., Turner, D.R., Lauer, A., Corbett, J.J., 2013. Shipping contributes to ocean acidification. Geophys. Res. Lett. 40 (11), 2731–2736. https://doi.org/10.1002/grl.50521.

Hunter, K.A., Liss, P.S., Surapipith, V., Dentener, F., Duce, R., Kanakidou, M., Kubilay, N., Mahowald, N., Okin, G., Sarin, M., Uematsu, M., Zhu, T., 2011. Impacts of anthropogenic SO_x, NO_x and NH_3 on acidification of coastal waters and shipping lanes. Geophys. Res. Lett. 38 (13). https://doi.org/10.1029/2011GL047720.

IPCC, 2007. In: Parry, M.L., Canziani, O.F., Palutikof, J.P., van der Linden, P.J., Hanson, C.E. (Eds.), Climate change 2007: Impacts, adaptation and vulnerability. Contribution of Working Group II to the Fourth Assessment Report of the Intergovernmental Panel on Climate Change. Cambridge University Press, Cambridge, UK, p. 976.

Isada, T., Hattori-Saito, A., Saito, H., Kondo, Y., Nishioka, J., Kuma, K., Hattori, H., McKay, R.M.L., Suzuki, K., 2018. Responses of phytoplankton assemblages to iron availability and mixing water masses during the spring bloom in the Oyashio region, NW Pacific. Limnol. Oceanogr. 64 (1), 197–216. https://doi.org/10.1002/lno.11031.

Ito, A., 2013. Global modeling study of potentially bioavailable iron input from shipboard aerosol sources to the ocean. Global Biogeochem. Cy. 27 (1), 1–10. https://doi.org/10.1029/2012GB004378.

Ito, A., Shi, Z.B., 2016. Delivery of anthropogenic bioavailable iron from mineral dust and combustion aerosols to the ocean. Atmos. Chem. Phys. 16 (1), 85–99. https://doi.org/10.5194/acp-16-85-2016.

Jagerbrand, A.K., Brutemark, A., Sveden, J.B., Gren, I., 2019. A review on the environmental impacts of shipping on aquatic and nearshore ecosystems. Sci. Total Environ. 695, 133637. https://doi.org/10.1016/j.scitotenv.2019.133637.

Jakuba, R.W., Saito, M.A., Moffett, J.W., Xu, Y., 2012. Dissolved zinc in the subarctic North Pacific and Bering Sea: its distribution, speciation, and importance to primary producers. Global Biogeochem. Cy. 26 (2). https://doi.org/10.1029/2010GB004004.
Jickells, T., An, Z., Andersen, K.K., Baker, A., Bergametti, G., Brooks, N., Cao, J., Boyd, P., Duce, R., Hunter, K., 2005. Global iron connections between desert dust, ocean biogeochemistry, and climate. Science. 308 (5718), 67–71. https://doi.org/10.1126/science.1105959.
Jickells, T.D., Buitenhuis, E., Altieri, K., Baker, A.R., Capone, D., Duce, R.A., Dentener, F., Fennel, K., Kanakidou, M., LaRoche, J., Lee, K., Liss, P., Middelburg, J.J., Moore, J.K., Okin, G., Oschlies, A., Sarin, M., Seitzinger, S., Sharples, J., Singh, A., Suntharalingam, P., Uematsu, M., Zamora, L.M., 2017. A reevaluation of the magnitude and impacts of anthropogenic atmospheric nitrogen inputs on the ocean. Global Biogeochem. Cy. 31 (2), 289–305. https://doi.org/10.1002/2016GB005586.
Kim, I.-N., Lee, K., Gruber, N., Karl, D.M., Bullister, J.L., Yang, S., Kim, T.-W., 2014. Increasing anthropogenic nitrogen in the North Pacific Ocean. Science. 346 (6213), 1102–1106. https://doi.org/10.1126/science.1258396.
Kitajima, S., Furuya, K., Hashihama, F., Takeda, S., Kanda, J., 2009. Latitudinal distribution of diazotrophs and their nitrogen fixation in the tropical and subtropical western North Pacific. Limnol. Oceanogr. 54, 537–547. https://doi.org/10.4319/lo.2009.54.2.0537.
Li, Q., Legendre, L., Jiao, N., 2015. Phytoplankton responses to nitrogen and iron limitation in the tropical and subtropical Pacific Ocean. J. Plankton Res. 37 (2), 306–319. https://doi.org/10.1093/plankt/fbv008.
Li, C., Borken-Kleefeld, J., Zheng, J., Yuan, Z., Ou, J., Li, Y., Wang, Y., Xu, Y., 2018. Decadal evolution of ship emissions in China from 2004 to 2013 by using an integrated AIS-based approach and projection to 2040. Atmos. Chem. Phys. 18 (8), 6075–6093. https://doi.org/10.5194/acp-18-6075-2018.
Liu, S., Zhang, J., Chen, S.Z., Chen, H., Hong, G., Wei, H., Wu, Q., 2003. Inventory of nutrient compounds in the Yellow Sea. Cont. Shelf Res. 23 (11), 1161–1174. https://doi.org/10.1016/S0278-4343(03)00089-X.
Liu, Y., Zhang, T., Shi, J., Gao, H., Yao, X., 2013. Responses of chlorophyll a to added nutrients, Asian dust, and rainwater in an oligotrophic zone of the Yellow Sea: implications for promotion and inhibition effects in an incubation experiment. J. Geophys. Res.-Biogeo. 118 (4), 1763–1772. https://doi.org/10.1002/2013JG002329.
Liu, H., Fu, M., Jin, X., Shang, Y., Shindell, D., Faluvegi, G., Shindell, C., He, K., 2016. Health and climate impacts of ocean-going vessels in East Asia. Nat. Clim. Chang. 6 (11), 1037–1041. https://doi.org/10.1038/nclimate3083.
Longhurst, A., Sathyendranath, S., Platt, T., Caverhill, C., 1995. An estimate of global primary production in the ocean from satellite radiometer data. J. Plankton Res. 17 (6), 1245–1271. https://doi.org/10.1093/plankt/17.6.1245.
Lv Z, Liu H, Ying Q, Fu M, Meng Z, Wang Y, Wei., W., Gong. H., He, K., 2018. Impacts of shipping emissions on PM2.5 pollution in China. Atmos. Chem. Phys. 18(21), 15811–15824. doi:https://doi.org/10.5194/acp-18-15811-2018.
Maranon, E., 2015. Cell size as a key determinant of phytoplankton metabolism and community structure. Annu. Rev. Mar. Sci. https://doi.org/10.1146/annurev-marine-010814-015955.
Martino, M., Hamilton, D., Baker, A.R., Jickells, T.D., Bromley, T., Nojiri, Y., Quack, B., Boyd, P.W., 2014. Western Pacific atmospheric nutrient deposition fluxes, their impact on surface ocean productivity. Global Biogeochem. Cy. 28 (7), 712–728. https://doi.org/10.1002/2013GB004794.
Measures, C., Cutter, G., Landing, W., Powell, R., 2006. Hydrographic observations during the 2002 IOC Contaminant Baseline Survey in the western Pacific Ocean. Geochem. Geophy. Geosy. 7. https://doi.org/10.1029/2004GC000855 Q03M06.
Meng, X., Chen, Y., Wang, B., Ma, Q., Wang, F., 2016. Responses of phytoplankton community to the input of different aerosols in the East China Sea. Geophys. Res. Lett. 43 (13), 7081–7088. https://doi.org/10.1002/2016GL069068.
Moore, C., Mills, M., Arrigo, K., Berman-Frank, I., Bopp, L., Boyd, P., Galbraith, E., Geider, R.J., Guieu, C., Jaccard, S., 2013. Processes and patterns of oceanic nutrient limitation. Nat. Geosci. 6 (9), 701–710. https://doi.org/10.1038/NGEO1765.
Noiri, Y., Kudo, I., Kiyosawa, H., Nishioka, J., Tsuda, A., 2005. Influence of iron and temperature on growth, nutrient utilization ratios and phytoplankton species composition in the western subarctic Pacific Ocean during the SEEDS experiment. Prog. Oceanogr. 64 (2), 149–166. https://doi.org/10.1016/j.pocean.2005.02.006.
Okin, G.S., Baker, A.R., Tegen, I., Mahowald, N.M., Dentener, F.J., Duce, R.A., Galloway, J.N., Hunter, K., Kanakidou, M., Kubilay, N., Prospero, J.M., Sarin, M., Surapipith, V., Uematsu, M., Zhu, T., 2011. Impacts of atmospheric nutrient deposition on marine productivity: roles of nitrogen, phosphorus, and iron. Global Biogeochem. Cy. 25 (2). https://doi.org/10.1029/2010GB003858.
Raudsepp, U., Maljutenko, I., Kõuts, M., Granhag, L., Wilewska-Bien, M., Hassellöv, I.M., Eriksson, K.M., Johansson, L., Jalkanen, J.P., Karl, M., Matthias, V., Moldanova, J., 2019. Shipborne nutrient dynamics and impact on the eutrophication in the Baltic Sea. Sci. Total Environ. 671, 189–207. https://doi.org/10.1016/j.scitotenv.2019.03.264.
Ren, J.L., Zhang, G.L., Zhang, J., Shi, J.H., Liu, S.M., Li, F.M., Jin, J., Liu, C.G., 2011. Distribution of dissolved aluminum in the southern Yellow Sea: influences of a dust storm and the spring bloom. Mar. Chem. 125 (1), 69–81. https://doi.org/10.1016/j.marchem.2011.02.004.
Saito, M.A., Goepfert, T.J., Ritt, J.T., 2008. Some thoughts on the concept of colimitation: three definitions and the importance of bioavailability. Limnol. Oceanogr. 53 (1), 276–290. https://doi.org/10.2307/40006168.
Schroth, A.W., Crusius, J., Sholkovitz, E.R., Bostick, B.C., 2009. Iron solubility driven by speciation in dust sources to the ocean. Nat. Geosci. 2 (5), 337–340. https://doi.org/10.1038/ngeo501.
Shi, J., Gao, H., Zhang, J., Tan, S., Ren, J., Liu, C., Liu, Y., Yao, X., 2012. Examination of causative link between a spring bloom and dry/wet deposition of Asian dust in the Yellow Sea, China. J. Geophys. Res.-Atmos. 117. https://doi.org/10.1029/2012JD017983 D17304.
Strickland, J.D.H., Parsons, T.R., 1972. A Practical Handbook of Seawater Analysis.
Turner, D.R., Edman, M., Gallego-Urrea, J.A., Claremar, B., Hassellov, I.M., Omstedt, A., Rutgersson, A., 2017. The potential future contribution of shipping to acidification of the Baltic Sea. Ambio. 1-11. https://doi.org/10.1007/s13280-017-0950-6.
UNCTAD, October 2019. Review of Maritime Transport 2019. New York. https://unctad.org/en/PublicationsLibrary/rmt2019_en.pdf.
Whitney, F.A., 2011. Nutrient variability in the mixed layer of the subarctic Pacific Ocean, 1987–2010. J. Oceanogr. 67 (4), 481–492. https://doi.org/10.1007/s10872-011-0051-2.
Yau, P.S., Lee, S.C., Corbett, J.J., Wang, C., Cheng, Y., Ho, K.F., 2012. Estimation of exhaust emission from ocean-going vessels in Hong Kong. Sci. Total Environ. 431, 299–306. https://doi.org/10.1016/j.scitotenv.2012.03.092.
Zhang, Y., Yang, X., Brown, R., Yang, L., Morawska, L., Ristovski, Z., Fu, Q., Huang, C., 2017. Shipping emissions and their impacts on air quality in China. Sci. Total Environ. 581, 186–198. https://doi.org/10.1016/j.scitotenv.2016.12.098.
Zhang, F., Chen, Y., Chen, Q., Feng, Y., Shang, Y., Yang, Gao, H., Tian, C., Li, J., Zhang, Gan, Matthias, V., Xie, Z., 2018a. Real-world emission factors of gaseous and particulate pollutants from marine fishing boats and their total emissions in China. Environ. Sci. Technol. 52 (8), 4910–4919. https://doi.org/10.1021/acs.est.7b04002.
Zhang, C., Gao H. W., Yao, X. H., Shi, Z. B., Shi, J. H, Yu, Y., Meng, L., Guo, X. Y., 2018b. Phytoplankton growth response to Asian dust addition in the Northwest Pacific Ocean versus the Yellow Sea. Biogeosciences, 15(3), 749–765. doi:https://doi.org/10.5194/bg-15-749-2018.
Zhang, J., Gao, Y., Leung, L.R., Luo, K., Liu, H., Lamarque, Fan J., Yao, X., Gao, H., Nagashima, T., 2019. Impacts of climate change and emissions on atmospheric oxidized nitrogen deposition over East Asia. Atmos. Chem. Phys. 19 (2), 887–900. https://doi.org/10.5194/acp-19-887-2019.
Zhang, C., Yao, X.H., Chen, Y., Chu, Q., Yu, Y., Shi, J.H., Gao, H.W., 2019a. Variations in the phytoplankton community due to dust additions in eutrophication, LNLC and HNLC oceanic zones. Sci. Total Environ. 669, 282–293. https://doi.org/10.1016/j.scitotenv.2019.02.068.
Zhang, C., Ito, A., Shi, Z.B., Aita, M.N., Yao, X.H., Chu, Q., Shi, J.H., Gong, X., Gao, H.W., 2019b. Fertilization of the Northwest Pacific Ocean by East Asia air pollutants. Global Biogeochem. Cy. 33 (6), 690–702. https://doi.org/10.1029/2018GB006146.
Zhang, F., Chen, Y., Tian, C., Lou, D., Li, J., Zhang, G., Matthias, V., 2020a. Emission factors for gaseous and particulate pollutants from offshore diesel engine vessels in China. Atmos. Chem. Phys. 16 (10), 6319–6334. https://doi.org/10.5194/acp-16-6319-2016.
Zhang, C., He, J.Y., Yao, X.H., Mu, Y.C., Guo, X.Y., Ding, X.K., Yu, Y., Shi, J.H., Gao, H.W., 2020b. Dynamics of phytoplankton and nutrient uptake following dust additions in the Northwest Pacific. Sci. Total Environ. 739, 139999. https://doi.org/10.1016/j.scitotenv.2020.139999.